



HAL
open science

LiFePO₄-ferri/ferrocyanide redox targeting aqueous posolyte: Set-up, efficiency and kinetics

Jose Vivo-Vilches, Arina Nadeina, Noura Rahbani, Vincent Seznec,
Dominique Larcher, Emmanuel Baudrin

► To cite this version:

Jose Vivo-Vilches, Arina Nadeina, Noura Rahbani, Vincent Seznec, Dominique Larcher, et al..
LiFePO₄-ferri/ferrocyanide redox targeting aqueous posolyte: Set-up, efficiency and kinetics. *Journal of Power Sources*, 2021, 488, pp.229387. 10.1016/j.jpowsour.2020.229387 . hal-03610942

HAL Id: hal-03610942

<https://u-picardie.hal.science/hal-03610942>

Submitted on 3 Feb 2023

HAL is a multi-disciplinary open access archive for the deposit and dissemination of scientific research documents, whether they are published or not. The documents may come from teaching and research institutions in France or abroad, or from public or private research centers.

L'archive ouverte pluridisciplinaire **HAL**, est destinée au dépôt et à la diffusion de documents scientifiques de niveau recherche, publiés ou non, émanant des établissements d'enseignement et de recherche français ou étrangers, des laboratoires publics ou privés.



Distributed under a Creative Commons Attribution - NonCommercial 4.0 International License

LiFePO₄-ferri/ferrocyanide redox targeting aqueous posolyte: set-up, efficiency and kinetics.

Jose Vivo-Vilches^{a-c}, Arina Nadeina^{a-c}, Noura Rahbani^{a-c}, Vincent Seznec^{a-c}, Dominique Larcher^{a-c}, Emmanuel Baudrin*^{a-c}.

^a Laboratoire de Réactivité et Chimie des Solides (LRCS), UMR CNRS 7374, Université de Picardie Jules Verne, 33 rue Saint-Leu, 80039 Amiens Cedex, France.

^b Institut de Chimie de Picardie (ICP), FR CNRS 3085, Amiens Cedex, France.

^c Réseau sur le Stockage Electrochimique de l'Energie (RS2E), FR CNRS 3459, France.

Abstract

Redox Targeting Redox Flow Batteries (RT-RFB), in which a solid insertion material reacts with soluble flowing active species (the mediators), were recently developed as alternative to the stellar vanadium technology. We have studied and optimized a posolyte having LiFePO₄ as solid material and ferri/ferro cyanide complexes as soluble mediator in DMSO/water solvent mixture. LiFePO₄ particles were shaped as dense pellets with controlled total porosity, obtained by Spark Plasma Sintering using NaCl microcrystals as hard template. The redox potential of the mediator couple was tuned by playing with the DMSO/water ratio in order to match the insertion/uptake potential of the solid. High reversibility and fast kinetics of the mediator/solid reaction were chemically assessed *ex-situ*. Electrochemical results under flow showed perfect reversibility, full reaction of the soluble mediator complex, and a linear increase in capacity of the posolyte with the quantity of added active solid. The best performances are obtained with 40 % porous pellets and at a current density of 0.25 mA.cm⁻². In these conditions, full capacity is reached for both the mediator and the solid material, with a first-cycle reversibility of 99%, doubling the capacity with only 1 vol% of added LiFePO₄ in the electrolyte.

Keywords: Redox flow battery, redox targeting, porous pellets, LiFePO₄, ferri/ferrocyanide.

*** corresponding author:** emmanuel.baudrin@u-picardie.fr

1. INTRODUCTION

One century after the Arrhenius's warnings [1], the worrying energetic situation prompts the urge to find alternative systems to store energy from renewable sources, such as solar and wind energies, intrinsically intermittent. Storage systems should i) have low environmental finger-prints, ii) enable easy and wide stationary implementation, and above all iii) have the ability to uncorrelate energy and power. To date, the most promising systems for such electrochemical applications are Redox Flow Batteries (RFBs) [2, 3, 4].

In a classical RFB, the electroactive species are not trapped in solid particles immobilized in solid electrodes as in Li-ion cells, but are dissolved in a liquid electrolyte. A full RFB thus consists of a positive active electrolyte (posolyte) and a negative active one (negolyte) stored in two separate tanks. The negolyte and posolyte are separately flown into the electrochemical cell where they exchange electrons collected by two electrodes (e.g. carbon foam/felt) separated by an ion-conducting membrane ensuring a specific ionic transfer of supporting electrolyte species but blocking the electroactive ones. This differs from classical batteries where the separator only acts as a physical barrier to avoid electrical contact between the solid electrodes. The amount of energy stored in a RFB (Wh) is proportional to i) the tanks volume, ii) the concentration of electro-active species, iii) the cell voltage and iv) the number of exchanged electrons per active species. The power of a RFB (W) is driven by the surface area of the electrodes/membrane and by the flow rate of the electrolytes through the electrochemical cell. RFB design also allows for several recharge options, e.g. refilling the tanks with new electrolytes [5], regenerating the electrolyte via external processes, or charging the cell by plugging it to the grid. Aside, many simple chemical, textural, physical and technical levers were proposed to tune both energy and power.

Many soluble redox couples were studied (e.g. $\text{Fe}^{3+}/\text{Fe}^{2+}$ or $\text{Cr}^{3+}/\text{Cr}^{2+}$) [6, 7], the most appealing being the vanadium-based system (VRFB) [8, 9]. It takes advantage of four soluble oxidation states of V (from +2 to +5), so that a single electrolyte could be used for both sides for the first charge of the cell, and this limits the consequences of a chemical cross-contamination through the membrane. Thanks to its relatively good reversibility, this technology is commercialized worldwide (up to several MW/unit) but it still suffers from the high and fluctuating cost of vanadium [10], high toxicity (V^{5+}) and acidity (>1 M) of the solutions, hydrogen evolution, and low volumetric/gravimetric energy density, the latter being mostly rooted in the limited concentration (1-2 mol.L⁻¹) of the active species, a general issue in RFBs. Attempts to increase this concentration using over-saturated solutions (> 2 M),

surfactants, mixed acids or additives generally resulted in a rise in viscosity [11] and long-term instability (precipitation). An apparently elegant approach to raise the specific energy is the use of flowing suspensions of active particles instead of solutions [12] but this “semi-solid” approach comes with abrasion issues and a large viscosity increase resulting from the need to use carbon additives to ensure electron percolation through the fluid [13]. These “semi-solid” RFBs should not be mistaken for the RFB technologies involving one static solid active electrode ($\text{Zn}^0/\text{bromide}$ [14]) or solid-state disproportionation reactions (e.g. $\text{Pb}^0/\text{PbO}_2/\text{Pb}^{2+}$).

In this context, another elegant concept also based on the use of Li (or Na) insertion materials emerged. Here, the solid particles are immobilized in the RFB tanks [15] or columns [16] where they will electrochemically react with dissolved redox mediators. This combines the advantage of the capacity gain brought by the semi-solid approach without the drawbacks of flowing suspensions. The dissolved species are doubly active: each one is oxidized/reduced at the cell level, and should then be able to react with its respective solid immersed in its related tank. This coined the term “Redox Targeting” Redox-Flow Battery (RT-RFB). The challenge is to find soluble mediators whose redox potentials target those of specific solid insertion materials. First, a setup using two different mediator molecules in each tank (one for oxidation, one for reduction) was proposed [17]. It was later found that a single mediator, whose potential is governed by Nernst’s law, would be enough if its redox potential is close enough to that of the insertion material [18, 19, 20]. Finally, a RT-RFB cumulates the energy resulting from the reaction between the flowing mediators themselves and that coming from the reaction between the two solids, mediated by the dissolved molecules. In this configuration, it is possible to obtain a bimodal power curve [21]. Since the concentration of active species in a solid is much higher than that in an electrolytic solution, the addition of solid insertion materials results in a neat increase in the volumetric energy density of RFBs. Recently, Yu et al. investigated a RT-RFB having $\text{LiFePO}_4/\text{LiTi}_2(\text{PO}_4)_3$ as solid active materials and TetraEthylene Glycol DiMethyl Ether (TEGDME) added to water to adjust the redox potential of the polysolite mediator ($\text{Fe}(\text{CN})_6^{3-} / \text{Fe}(\text{CN})_6^{4-}$) [22].

Following the same approach, we focused here on the polysolite side with: LiFePO_4 (LFP) as active material, $[\text{Fe}(\text{CN})_6]^{3-} / [\text{Fe}(\text{CN})_6]^{4-}$ as mediator redox couple, and a mixture of dimethyl sulfoxide (DMSO) and water as solvent. LFP powder was shaped into thick porous pellets prepared by leaching out NaCl from NaCl/LFP/Carbon dense pellets made using SPS (Spark Plasma Sintering) [23, 24]. The influence of varying experimental conditions such as current density, powder loading, and pellet porosity on the overall electrochemical response

(reversibility, polarization, volumetric capacity, percentage of reacted solid) was assessed, as well as the kinetics of the mediated (de)insertion reactions.

2. Experimental section

2.1 *LiFePO₄ and pellets preparation (SPS)*

LiFePO₄ (LFP) porous pellets were prepared using Spark Plasma Sintering (SPS) and a hard templating route as described in previous studies [24]. Initial intimate LFP (coated with 1.8 % carbon) and NaCl (Sigma-Aldrich, $\geq 99.5\%$) mixtures were prepared by ball-milling (30 min, SPEX Mixer Mill 8000M, 1725 rpm, three stainless steel balls for 450 mg of LFP/NaCl mixture) obtaining powders with two different LFP/NaCl volume ratios (70/30 and 60/40). Ball-milled mixtures were packed in graphite dies (internal diameter 10 mm, target mass of each pellet: 450 mg) lined with graphite paper and compacted for 5 min under 4 tons.cm⁻² at room temperature. Then, each graphite die was placed in the SPS chamber and a sintering procedure was performed by the following protocol: cold-pressing (at room temperature) at 4 kN for 5 min, heating/cooling (60°C/min), pressing (0.6 kN/min), dwelling plateau (600 °C, 10 kN – 5 min). As-obtained pellets were polished with sandpaper down to approximately 1 mm thickness. Leaching of NaCl from these pellets was achieved by soaking them in distilled water (circa 50 mL per pellet) for a few hours and changing water regularly until chloride could not be detected anymore in the solution (no AgCl precipitation after addition of Ag⁺ solution). The pellets were dried at 80°C overnight and the efficiency of the NaCl removal was evaluated by weight-loss calculations along with X-Ray Diffraction measurements. Pellets were labeled LFP30NaCl and LFP40NaCl, in reference to their volumetric NaCl contents (30 and 40 vol%), while leached pellets were accordingly named LFP30 and LFP40.

2.2 Physicochemical characterization

X-ray diffraction (XRD) patterns were obtained with a D8 diffractometer (Bruker) using a Cu K α ($\lambda=1.5406$ Å) radiation. SEM images and elemental analysis of samples (before and after NaCl leaching) were taken using an FEI Quanta 200F field emission SEM equipped with an Oxford EDX spectrometer. Densities were evaluated by helium pycnometry (AccuPyc 1330, Micromeritics) at room temperature and using high purity dry He (> 99.99 %). Before measurements, samples (> 1 g) were flushed with He. Each result is the mean value of 5 consecutive analyses, with deviation generally lower than 0.5 %.

2.3 Electrochemical measurements

Cyclic voltammetry (CV) and Chronoamperometry (CA) experiments were performed in a 3-electrodes setup, employing a Pt foil as working electrode, a graphite paper as counter electrode and Hg/Hg₂SO₄ as reference electrode. The three electrodes were connected to a VSP potentiostat (Biologic Instrument).

All potentials are reported with respect to the SHE electrode

2.3.1 Preparation and study of the posolyte.

Posolyte solutions were prepared by dissolving potassium ferro-cyanide K₄Fe(CN)₆ (Fe²⁺ complex, Sigma-Aldrich) and potassium ferri-cyanide K₃Fe(CN)₆ (Fe³⁺ complex, Sigma-Aldrich) in a mixture of dimethyl sulfoxide (DMSO, VWR) and distilled water. LiCl was added to all the solutions at the same concentration (0.5 M), both as a Li⁺ source and a supporting electrolyte.

For the kinetic experiments, 200 mg of pellets were immersed in 50 mL of 0.1 M [Fe(CN)₆]³⁻ electrolyte and 0.5 M LiCl in DMSO/water (20/80 vol./vol.). Then, aliquots of the supernatant (100 μL) were withdrawn at different times and diluted (with 0.5 M LiCl in a DMSO/water (20/80 vol./vol.) mixture) in 10 mL volumetric flasks. UV-VIS spectra were collected using an Agilent Cary 5000 UV-Vis-NIR spectrophotometer and a quartz cuvette. The concentration in [Fe(CN)₆]³⁻ was determined from the absorbance measured at 420 nm after a proper calibration. Standard solutions of 0 to 1 mM [Fe(CN)₆]³⁻ were prepared by dissolving K₃Fe(CN)₆ in a solution of LiCl (0.5 M) in a DMSO/water (20/80 vol./vol.) mixture.

2.3.2 Redox-Flow Battery set-up

The core of our RFB setup is a commercial Flow Cell (CFLOW 5x5) with 25 cm² electrodes and current collectors (Fig. 1B). Commercial carbon felt (Alfa-Aesar) electrodes were pre-oxidized in air (400 °C, 30 hours) prior to use in order to increase their water-wettability. A Nafion ion-exchange membrane (NRE-212 0.05 mm thick, Alfa-Aesar), preconditioned in LiCl 0.5 M, was placed between the two half cells, which were connected to their respective electrolyte tanks by a homemade tubing setup. A peristaltic pump (Watson

Marlow 323) enables the circulation of the solutions through the cell/tubes with a constant and calibrated flow. The electrolyte tanks (Fig. 1A) were placed in a thermostatic bath, and a separate container hosting the solid/pellets (Fig. 1C) was connected on the track of the posolyte tubing (Fig. 1). Solutions of $\text{K}_4\text{Fe}(\text{CN})_6$ and $\text{K}_3\text{Fe}(\text{CN})_6$ (0.2 M in DMSO/water + 0.5 M LiCl) were loaded into the posolyte and negolyte tanks, respectively. Each tank has a 250 mL total capacity. A larger volume of negolyte (180 mL vs. 60 mL) ensures that the capacity of the cell is only limited by the positive side so that the effect of adding LFP could be observed. Galvanostatic experiments were performed at current densities ranging from 0.25 to $1 \text{ mA}\cdot\text{cm}^{-2}$ using a VSP potentiostat.

In order to obtain reliable results on the targeting reaction between LFP and the ferri/ferro-cyanide mediator, the electrochemical setup had to be optimized. The first option for immobilizing the material outside the electrochemical cell while keeping it in contact with the circulating electrolyte was to block some LFP powder between two paper-stoppers in a connection tube between the posolyte tank and the electrochemical cell. However, this setup was unsuccessful due to the progressive compaction of the powder as the experiments proceeded, leading to difficulties to control i) the electrolyte flow, and ii) the evolving porosity of the powder. This led to the second setup, which relies on the fabrication and use of dense porous pellets, in line with previous work from Qin Wang's group [22] where polymeric based granules were added inside the tank (note, however, that no precise description of the granule preparation was reported). Another factor to consider is the location of the solid material in the circuit, as it has a crucial impact on the functioning of the system, maximizing the concentration of active species in contact with the solid material. At any time of the process, the volume of electrolyte present in the tubing is much lower than the volume of electrolyte standing in the tank. As a consequence, during charging, the ferric species formed at the cell level undergo a drastic dilution when reaching the reserve tank (assuming that during operation 30 mL of the electrolyte is present in the tubing and the other 30 mL is in the tank) and their concentration may then become too low to efficiently oxidize LFP as we observed experimentally. So, the solid material should be held between the cell and the posolyte reservoir, for it to react with the mediator before any possibility of dilution within the main tank. Finally, we observed that the reaction between the ferric species and LFP pellets is favored if they are placed in a container where they are always in contact with a small volume of the electrolyte (see Figure 1).

3. RESULTS AND DISCUSSION

Porous pellets preparation and characterization

Initially developed for the preparation of thick porous electrodes for Li-Ion batteries [24], we implemented the use of SPS to prepare porous pellets with controlled porosity for redox-flow testing. The principle is to prepare by SPS a dense pellet made of LFP with a porogen (NaCl) in a fixed volumetric ratio and to subsequently dissolve this porogen. After ball milling the NaCl/LFP mixture and SPS pressing, 1 mm thick pellets were obtained. The theoretical densities ($\rho_{\text{theor.}}$) of the pellets can be calculated from the skeletal (pycnometry) densities of LFP ($\rho = 3.51 \text{ g.cm}^{-3}$) and of NaCl ($\rho = 2.14 \text{ g.cm}^{-3}$) and their volumetric ratio. These $\rho_{\text{theor.}}$ were compared to the apparent geometrical densities ($\rho_{\text{app.}}$) of the pellets (**Table 1**), calculated as the ratio of their measured mass over their measured geometric volume. The total porosity (closed + accessible) of the pellets can hence be computed from these two density values. All these data are compared in **Table 1**. For each composition, the reported values are the average for ten different samples, data from which a confidence interval can also be extracted. Clearly, the porosity of the non-leached samples (LFP30NaCl and LFP40NaCl) is around 10 %, meaning that the SPS technique produces pellets with 90 % compactness. Note that this initial porosity may be open porosity or not. After NaCl leaching, total porosity increases up to 36 % (LFP30) and 47 % (LFP40) in average. So, the increases in open porosity due to the NaCl dissolution (27 % and 35 %) are in good agreement with the initial NaCl volumetric contents (30 % and 40 %).

The SEM pictures (**Figure 2**) clearly show that macropores are generated during NaCl removal, in agreement with the micronic size of the NaCl crystals as illustrated by the samples LFP30 and LFP30NaCl. The pore size is not altered when the NaCl content is raised (LFP30 \rightarrow LFP40), but the number of pores appears to be substantially higher (**Figures 2c-d**). EDS mapping (**Figure SI 1a-b**) and elemental analysis (**Figure SI 1c-d**) confirm that shape/size of regions where Na is concentrated (LFP30NaCl) are in a good agreement with the shape/size of the pores created during the leaching (LFP30), and that no sodium or chlorine could be anymore detected after leaching, demonstrating a very efficient template removal.

The XRD pattern for the initial LFP powder (**Figure 3a**) is characteristic of well crystallized LiFePO_4 phase without any **crystalline** impurity. The calculated cell parameters (a

= 10.3246 Å; b = 6.0043 Å; c = 4.6916 Å) as well as the relative peaks intensities are in good agreement with previous reports [25]. The XRD pattern of LFP30NaCl (**Figure 3b**) logically exhibits two additional diffraction peaks corresponding to cubic NaCl (at about 27.5 ° and 32 °2θ), together with a small peak related to a KBr impurity (at ca. 29 °2θ) in the used sodium chloride. In agreement with our EDS analysis, these three peaks are not present anymore in the XRD pattern of LFP30 (**Figure 3b**), which is very similar to that of the initial LFP powder.

All these experiments show that the washing treatment is effective to remove completely the solid template (NaCl), that the SPS and leaching steps do not alter the LFP material (at least from XRD data), and that the overall procedure successfully produces self-standing macroporous pellets with controlled volume of open porosity. This last point is crucial in view of controlling the amount of surface of the active material that will be exposed to the electrolytic solution in the battery.

Thermodynamics and Kinetics of the reaction between (Li)FePO₄ and [Fe(CN)₆]^{3-/4-}

One of the key points of the present strategy is to tune the redox potential of a single mediator in such a way that its oxidized form is able to react with the reduced form of the solid material and vice versa, instead of using two different mediators (one for the oxidation, one for the reduction of the insertion material). In many cases, this is a tricky and long task but, fortunately, some strategies can be applied to notably shift the redox potential of a given mediator towards desired values. Among them, the use of mixed solvents is very efficient [22]. It is based on the differences in the solvent donor/acceptor properties with namely a decrease of the redox potential when the acceptor number decreases [26]. This is illustrated in **Figure 4** depicting the evolution of the CV signal for [Fe(CN)₆]⁴⁻ solutions in DMSO/water mixtures used for the fine tuning of the potential (the acceptor numbers are 19.5 and 54.8 for DMSO and water, respectively, [26]). Clearly, the CV curves are monotonously shifted to lower voltages as the volumetric percentage of DMSO increases (**Figure 4a**) and the formal potential (E°) follows a linear decrease with the DMSO content (**Figure 4b**). The redox potential for the FePO₄/LiFePO₄ couple lies at $E = 0.37$ V vs. SHE in our conditions (0.5 M Li⁺) [22]. So, in order to have a good match between this potential and that of the mediator, we must use a solvent mixture **with a 20:80 volumetric ratio (DMSO:H₂O)**.

In order to confirm this point, we conducted a series of experiments consisting in which porous LFP pellets were soaked in DMSO/water solutions of the above composition and containing different $[\text{Fe}(\text{CN})_6]^{3-} / [\text{Fe}(\text{CN})_6]^{4-}$ ratios and 0.5 M LiCl as supporting electrolyte and source of Li^+ . The total Fe concentration was fixed to 0.05 M, and 100 mL of each solution reacted with two LFP30 pellets (≈ 200 mg) for 48 h. In these conditions, there is a large excess (≈ 4 times) of mediator species in solution with respect to the redox centers in the solid. After each experiment, the pellets were rinsed with distilled water, dried, and an XRD pattern collected. According to Nernst's equation, the formal potential (E°) for the $[\text{Fe}(\text{CN})_6]^{3-} / [\text{Fe}(\text{CN})_6]^{4-}$ couple, as plotted in **Figure 4a**, is reached in equimolar conditions, i.e. $[\text{Fe}(\text{CN})_6]^{3-} / [\text{Fe}(\text{CN})_6]^{4-} = 1$. Therefore, it is expected that oxidation of LFP only occurs when the concentration of $[\text{Fe}(\text{CN})_6]^{3-}$ is larger than that of $[\text{Fe}(\text{CN})_6]^{4-}$, while FP reduction should be observed when there is an excess of the reduced $[\text{Fe}(\text{CN})_6]^{4-}$ form, which is reflected in our experimental results, when looking qualitatively at the evolution of the XRD reflections intensities for both phases. First, when LFP30 pellets react with solutions having low (0, 25 or 50 %) $[\text{Fe}(\text{CN})_6]^{3-}$ contents (**Figure 5a-b**), XRD patterns were unchanged. Then, FePO_4 diffraction peaks start to appear when the material reacted with a solution containing 75 % $[\text{Fe}(\text{CN})_6]^{3-}$ clueing a partial oxidation of the material. Full oxidation of LFP into FP was completed after reacting with solution having 100 % $[\text{Fe}(\text{CN})_6]^{3-}$. The reverse sequence of events is observed for the reduction of FP while increasing the concentration of $[\text{Fe}(\text{CN})_6]^{4-}$ (**Figure 5c-d**), with no evidences of the reaction for the experiments where the proportion in $[\text{Fe}(\text{CN})_6]^{4-}$ was 0, 25 or 50 %, LFP being formed back from FP when using solutions having 75 % $[\text{Fe}(\text{CN})_6]^{4-}$ and the full reaction is observed for 100 % $[\text{Fe}(\text{CN})_6]^{4-}$ solution.

The above results confirm the thermodynamic control of the reaction between the active material in the pellet and the mediator species, however, the kinetics of this reaction have to be explored since we observed that the reaction may not be complete after 48 h of contact between the pellet and the solution. In a RT-RFB, the cell voltage is related to the state of charge of the solution, and the additional capacity supplied by the insertion material would be limited by the kinetics of the reaction between the solid and the mediator. This prompted us to study this in our system. $[\text{Fe}(\text{CN})_6]^{3-}$ exhibits a unique UV-Vis absorption maximum at 420 nm, which enables us to follow the drop in $[\text{Fe}(\text{CN})_6]^{3-}$ concentration in the electrolyte as a function of contact time with the LFP30 pellets. From this evolution, the amount of generated FePO_4 can be computed as well. Experiments were conducted by

soaking $2 \cdot 10^{-3}$ mole of LFP30 in 50 mL of electrolyte. Two electrolytes (A and B) having two different states of charge were tested: electrolyte A contains only $\text{Fe}(\text{CN})_6^{3-}$ (100 mM), and electrolyte B contains 60 mM $\text{Fe}(\text{CN})_6^{3-}$ + 40 mM $\text{Fe}(\text{CN})_6^{4-}$. To mimic the real conditions of battery cycling, the mediator solution was circulated over the solid at a flow rate of 30 $\text{mL} \cdot \text{min}^{-1}$. The results (**Figure 6**) show that LFP oxidation is quite fast when using electrolyte A: 64 % of the reaction is completed after ca. 5 hours, with a maximum final yield (30 h) of around 78 %, the unreacted 22 % probably corresponding to the inner part of the pellets which is inaccessible to the electrolyte. The negative impact of a low state of charge of the electrolyte is underlined by the experiment performed with electrolyte B: the reaction is also fast along the first hours, but the maximum final yield of oxidation reaches only 14 % after 30 hours. All these results are consistent with the evolution in XRD and in potential as a function of the $[\text{Fe}(\text{CN})_6]^{3-} / [\text{Fe}(\text{CN})_6]^{4-}$ ratio (**Figure 5**). It emphasizes that the reaction is mostly thermodynamically controlled, and that the concentration of the oxidized mediator should be therefore maintained as high as possible. This condition will be met in a real-life RT-RFB where the charge process will regenerate this oxidized form at the cell level with homogeneity obtained within the flow. It also explains that the position of the pellets within the flow as adapted in the present work (**Figure 1**) is important. These results also suggest that pellets with higher porosity (> 30%) should be prepared and tested in order to lower the non-accessible part of the solid we detected above ($\approx 22\%$).

Redox Flow Battery half-cell test of targeting reaction.

Using our setup (**Figure 1**) and optimized conditions (negolyte in excess, solvent composition ...), we first tested the electrochemical behavior of the electrolyte alone (0.2 M $\text{Fe}(\text{CN})_6^{4-}$ in DMSO/ H_2O (20/80 vol/vol) + LiCl 0.5 M) in galvanostatic mode at 1 $\text{mA} \cdot \text{cm}^{-2}$. This assured (**Figure 7a, black curve**) that this system is fully reversible and that its capacity matches the theoretical one (322 mAh, 0.012 mole, **Table 2**). The experiment was then repeated with the addition of 1.85 g of LFP30 pellets. This led to a clear rise in capacity (+170 mAh for the charge) (**Figure 7a, green curve**), meaning that 54 % of the LFP is active (**Table 2**). Note that this is in the same range that was reported by Yu et al. [22] for a similar material but processed in a different way and with a different solvent mixture. Nevertheless, the reaction was showing a much lower first-cycle reversibility (85%) than for the sole mediator ($\sim 100\%$). In order to favor the solid/electrolyte percolation and the surface of contact, LFP40 pellets with a larger volume of pores were tested (**Figure 7b**). This had a small impact

on the proportion of active solid material oxidized during the charge (45 % vs. 54 % for LFP30), but the first-cycle reversibility was considerably improved (96 % vs. 85% for LFP30). Note that these results are different from our kinetic results (LFP30, **Figure 6b**) due to the difference of protocol. Indeed, in **Figure 6**, the electrolyte A (100% $[\text{Fe}(\text{CN}_6)]^{3-}$) is at a 100 % SOC(State of Charge), while we are here much closer to an applicable situation with a flowing electrolyte which is under charge (the oxidation occurs only above 50% SOC of the mediator solution)

In such RT-RFB, the threshold step is the targeting reaction with coupled charge transfer at the solid/electrolyte interface and lithium diffusion in the solid. A lower current density should thus give more time for the material to react with the solution, so that both the proportion of active material and the reversibility could be possibly enhanced. This is what we observe when we compare the cycling data recorded at $1 \text{ mA}\cdot\text{cm}^{-2}$ and $0.25 \text{ mA}\cdot\text{cm}^{-2}$ (**Figure 7b**). At $0.25 \text{ mA}\cdot\text{cm}^{-2}$, we almost reach the theoretical capacity (656 mAh vs. 660 mAh), meaning that almost (99 %) all of the added solid (LFP40) reacted with the oxidizing mediator generated in the electrochemical cell (**Table 2**). Moreover, the first-charge coulombic efficiency of the system reaches 99%. Therefore, under these conditions, we were able to increase the capacity in an effective way (i.e. a high percentage of utilization of the added solid) with a very good reversibility.

One of the greatest advantages of the redox targeting is the increase in volumetric capacity due to the larger density of redox centers in solids with respect to solutions (“solid booster” according to Zanzola et al. [19]). To illustrate this, charge-discharge experiments with different added loadings of LFP40 were performed at 0.25 and $1.00 \text{ mA}\cdot\text{cm}^{-2}$, with the objective of clearly quantifying the gain in capacity as a function of the volume occupied by the added solid in the tank. (**Figure 8**). As expected, the capacity related to the solid/electrolyte reaction linearly increases with the percentage of volume occupied by the solid in the tank. Furthermore, the slope is clearly higher for the experiments run at $0.25 \text{ mA}\cdot\text{cm}^{-2}$ than for $1 \text{ mA}\cdot\text{cm}^{-2}$. Quantitatively, adding 1% vol. of LFP in the electrolyte increases the total capacity by $\approx 30 \%$ at $1 \text{ mA}\cdot\text{cm}^{-2}$, and up to $\approx 50 \%$ at $0.25 \text{ mA}\cdot\text{cm}^{-2}$. In other words, the total capacity of the posolyte is doubled when 1 % of LFP is added to the electrolyte.

4. Conclusions

A polysolite for Redox Targeting based RFB composed by LFP and potassium ferrocyanide was successfully prepared. Thermodynamic and kinetic studies of the targeting reaction revealed the importance of maximizing the concentration of the active species in solution. Therefore, a setup in which a sample holder was placed between the battery and the electrolyte tank was built, since it is here where this concentration reaches its maximum value at a given time. Furthermore, LFP was processed by SPS, since using the material in the form of powder was not convenient for a flow system. Samples with different porosities were prepared, demonstrating the importance of this property, specially for a correct reduction of the solid material during the discharge through lithiation.

The understanding of the targeting reaction at play allowed for designing and testing an RT-RFB system based on $\text{LiFePO}_4/\text{FePO}_4$ and $[\text{Fe}(\text{CN})_6]^{3/4-}$ that maximizes the capacity and the reversibility of the charge/discharge process. Under the specific conditions of low current density and a very porous material, we were able to achieve a capacity close to the theoretical one for the system and with a very high coulombic efficiency of 99%, which are improvements on the results currently found in the literature. The electrochemical results of the tested half-cell illustrate the importance of material processing in controlling and optimizing the performance of a RT-RFB alongside the influence of other variables such as the current density. This allowed us to build an efficient system with large capacity and high coulombic efficiency under selected conditions. While the current work could be taken as a proof of concept for the impact of material processing and cell design on the performance of RT-RFBs, the scope could be extended to larger scale optimizations and to a wider selection of mediator/insertion material couples.

5. Acknowledgments

The region Hauts-de-France is gratefully acknowledged for financial support through the “Renforcement du stockage de l’énergie” project and grant accorded to J V-V.

References

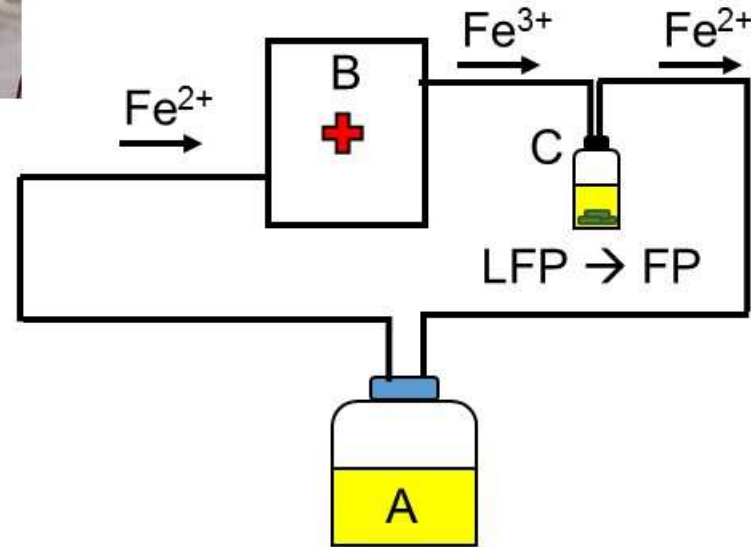
- [1] S. Arrhenius, “Conférences sur quelques problèmes actuels de la chimie physique et cosmique”, Ed. Gauthier-Villars, Paris (1922)
- [2] A.Z. Weber, M.M. Mench, J.P. Meyers, P.N. Ross, J.T. Gostick, Q. Liu, Redox-flow batteries: a review, *J. Appl. Electrochem.*, 41 (2011) 1137.
- [3] C. Ponce de Leon, A. Frias-Ferrer, J. Gonzalez-Garcia, D.A. Szanto, F.C. Walsh, Redox-flow cells for energy conversion, *J. of Power Sources* **160** (2006) 716-732.
- [4] T.M. Gür, Review of electrical energy storage technologies, materials and systems: challenges and prospects for large-scale grid storage, *Energy Environ. Sci.*, 11 (2018) 2696-2767.
- [5] J. Williams, Maritime batteries: a growth opportunity, IFBF 2020, Webinar.
- [6] J. Noack, N. Roznyatovskaya, T. Herr, P. Fischer, The chemistry of redox-flow batteries, *Angew. Chem. Int. Ed.*, 54 (2015) 9776-9809.
- [7] M. Bartolozzi, Development of redox flow batteries. A historical bibliography, *J. Power sources*, 25 (1989) 219-234.
- [8] E. Sum, M. Skyllas-Kazacos, A study of the V(II)/V(III) redox couple for redox-flow cell applications, *J. Power Sources*, **15** (1985) 179-190; E. Sum, M. Rychcik, M. Skyllas-Kazacos, Investigation of the V(V)/V(IV) system for use in the positive half-cell of a redox battery, *J. Power Sources*, 16 (1985) 85-95.
- [9] M. Skyllas-Kazacos, M. Rychcik, R. Robins, All-vanadium redox battery, US Patent 4,786,567 (November 1988)
- [10] M. Petranikova, A.H. Tkaczyk, A. Bartl, A. Amato, V. Lapkovskis, C. Tunsu, Vanadium sustainability in the context of innovative recycling and sourcing development, *Waste Management*, in press (<https://doi.org/10.1016/j.wasman.2020.04.007>)
- [11] F. Rahman, M. Skyllas-Kazacos, Optimization of supersaturated vanadium electrolyte for high energy density vanadium redox battery, Proceedings of the 4th Chemistry in Industry Conference & Exhibition, Bahrain, 2000
- [12] M. Duduta, B. Ho, V.C. Wood, P. Limthongkul, V.E. Brunini, W.C. Carter, Y.-M. Chiang, Semi-solid lithium rechargeable flow battery, *Adv. Energy Mater.*, **1** (2011) 511-516.
- [13] H. Parant, G. Muller, T. Le Mercier, J.-M. Tarascon, P. Poulin, A. Colin, Flowing suspensions of carbon black with high electronic conductivity for flow applications: comparison between carbon black and exhibition of specific aggregation of carbon particles, *Carbon* 119 (2017) 10-20.
- [14] Lim H.S., Lackner A.M., Knechtli R.C., Zinc-Bromine Secondary Battery, *J. Electrochem. Soc.*, **124(8)** (1977) 1154

-
- [15] Q. Huang, H. Li, M. Grätzel, Q. Wang, Reversible chemical delithiation/lithiation of LiFePO_4 : towards a redox flow lithium-ion battery, *Phys. Chem. Chem. Phys.*, 15 (2013) 1793-1797.
- [16] K. Camman, Towards a new generation of Redox-flow batteries, quoted as Ref [102] in L.F Arenas. C. Ponce de Leon, F.C. Walsh, Engineering aspects of the design, construction and performance of modular redox flow batteries for energy storage, *J. Energ. Storage*, 11 (2017) 119-153.
- [17] C. Jia, F. Pan, Y.G. Zhu, Q. Huang, L. Lu, Q. Wang, High-energy density nonaqueous all redox flow lithium battery enabled with a polymeric membrane, *Sci. Adv.* 1(10) (2015) e150886.
- [18] M. Zhou, Q. Huang, T.N. Truong, J. Ghilane, Y.G. Zhu, C. Jia, R. Yan, H. Randriamahazaka, Q. Wang, Nernstian-potential driven redox-targeting reactions of battery materials, *Chem.* 3 (2017) 1036-1049.
- [19] E. Zanzola, C.R Dennison, A. Battistel, P. Peljo, H. Vrubel, V. Amstutz, H.H. Girault, Redox solid energy boosters for flow batteries: polyaniline as a case study, *Electrochimica Acta* 235(2017) 664-671.
- [20] T. Paez, A. Martinez-Cuezva, J. Palma, E. Ventosa, Mediated alkaline flow batteries: from fundamentals to application, *ACS Appl. Energy Mater.* 2 (2019) 8328-8336.
- [21] Y. Chen, M. Zhou, Y. Xia, X. Wang, Y. Liu, Y. Yao, H. Zhang, Y. Li, S. Lu, W. Qin, X. Wu, Q. Wang, A stable and high-capacity redox targeting-based electrolyte for aqueous flow batteries, *Joule* 3(9) (2019) 2255-2267.
- [22] J. Yu, L. Fan, R. Yan, M. Zhou, Q. Wang, Redox-targeting-based aqueous redox flow lithium battery, *ACS Energy Lett.* 3 (2018) 2314-2320.
- [23] C. Gaillard, J.F. Despois. A. Mortensen, Processing of NaCl powders of controlled size and shape for the microstructural tailoring of aluminium foams. *Mater. Sci. Eng. A* 374 (2004) 250-262.
- [24] R. Elango, A. Demortière, V. De Andrade, M. Morcrette, V. Seznec, Thick Binder-Free Electrodes for Li-Ion Battery Fabricated Using Templating Approach and Spark Plasma Sintering Reveals High Areal Capacity. *Adv. Energy Mater.* 8 (2018) 1703031.
- [25] G. Rousse, J. Rodriguez-Carvajal, S. Patoux, C. Masquelier, Magnetic structures of the triphylite LiFePO_4 and of its delithiated form FePO_4 , *Chem. Mater* 15(21) (2003) 4082-4090.
- [26] V. Gutmann, Empirical parameters for donor and acceptor properties of solvents, *Electrochim. Acta*, 21 (1976) 661-670; V. Gutmann, G. Gritzner, K. Danksagmüller, Solvent effects on the redox potential of hexacyanoferrate(III)-hexacyanoferrate(II), *Inorg. Chim. Acta*, 17 (1976) 81-86.

B



C



A

Figure 1

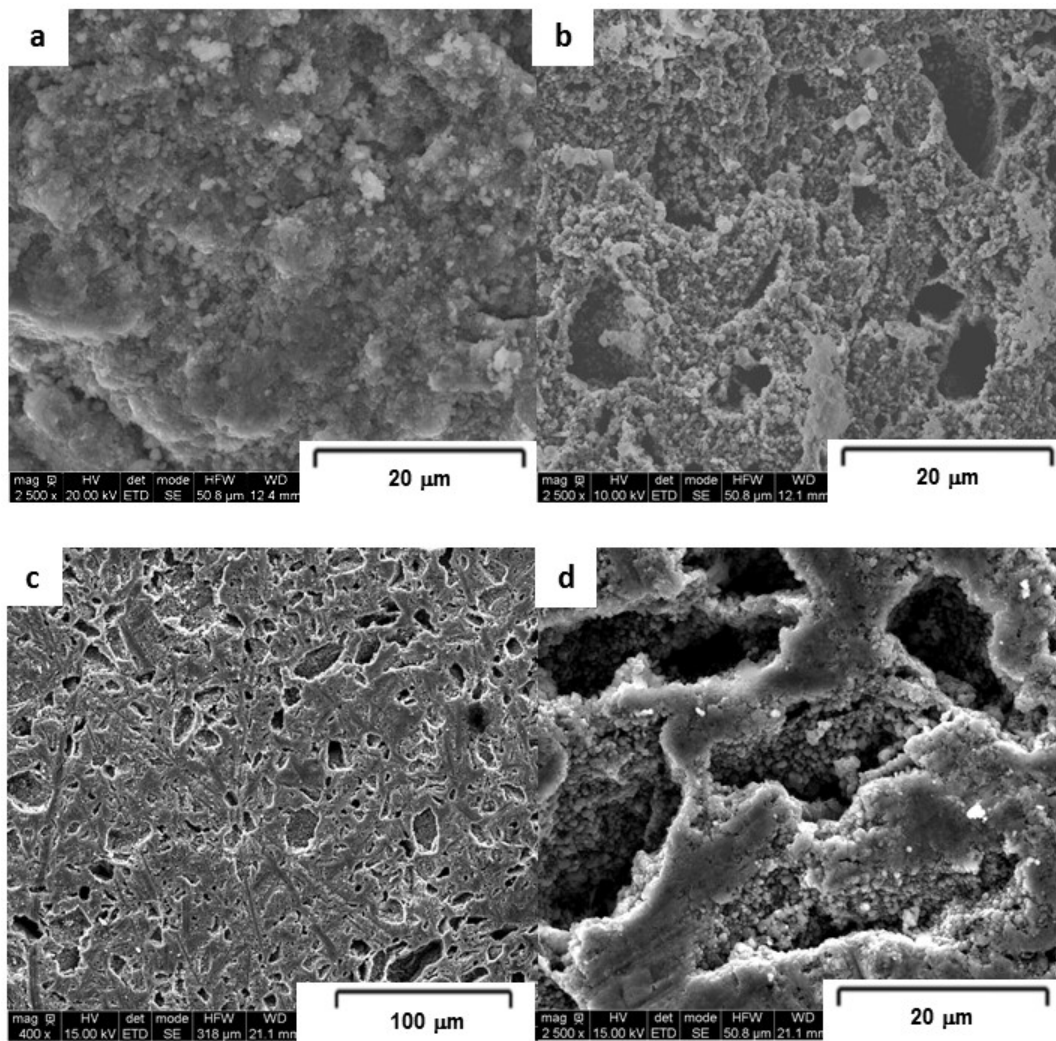


Figure 2

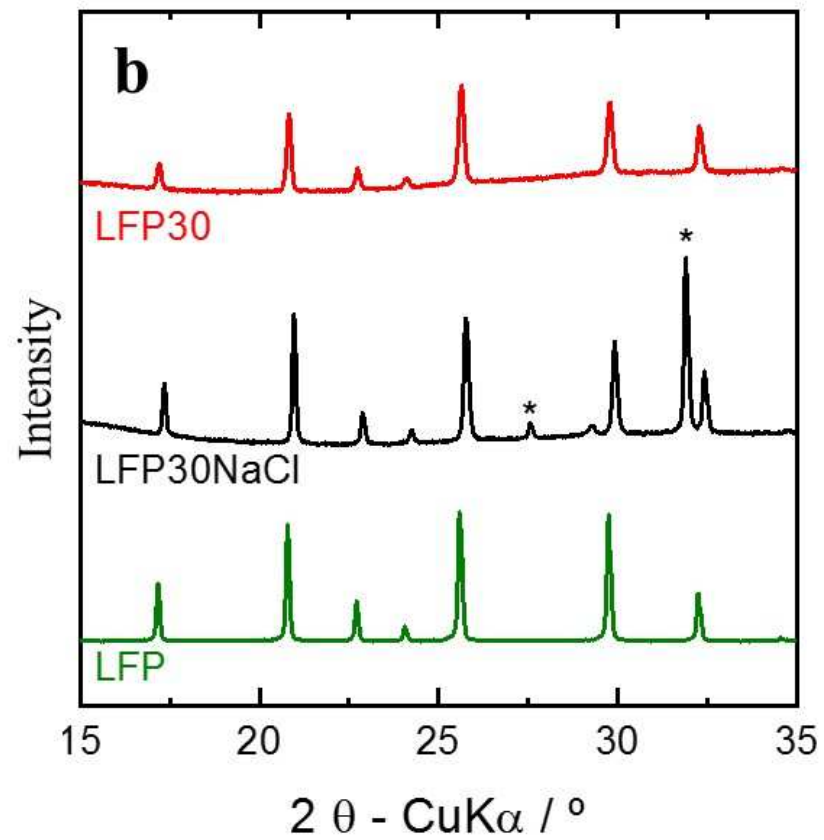
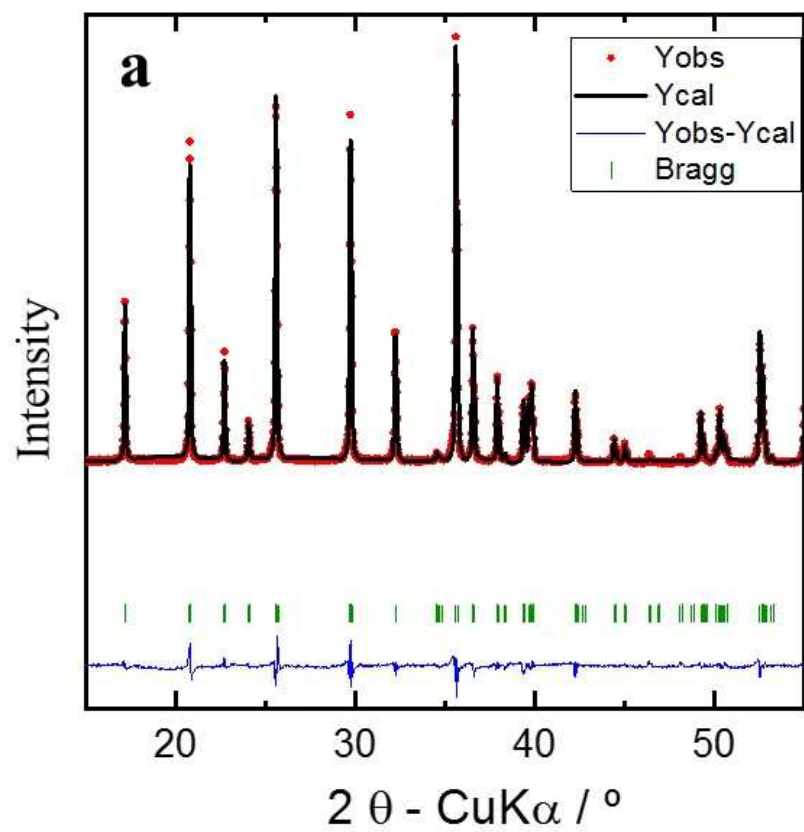


Figure 3

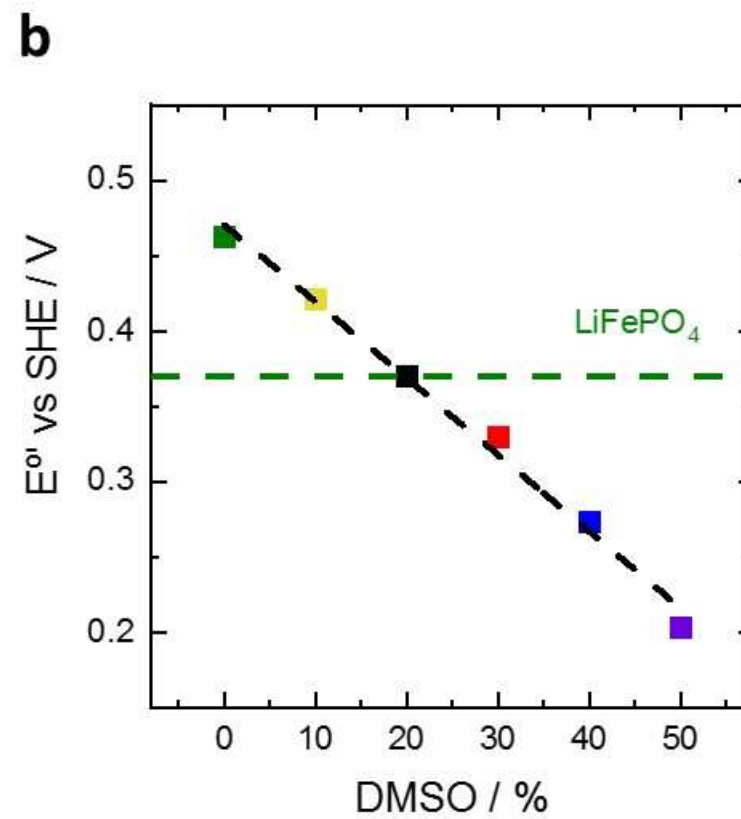
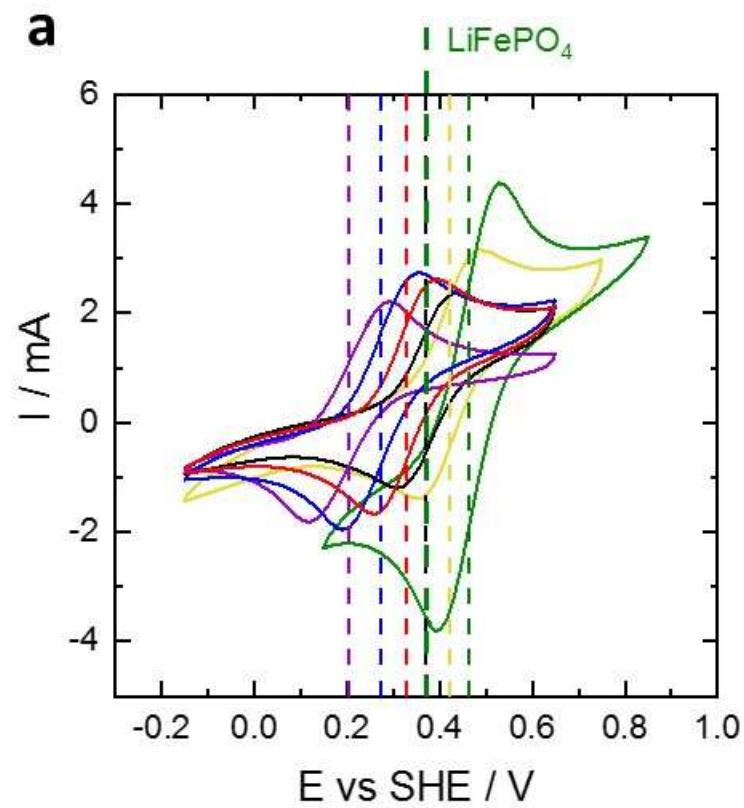


Figure 4

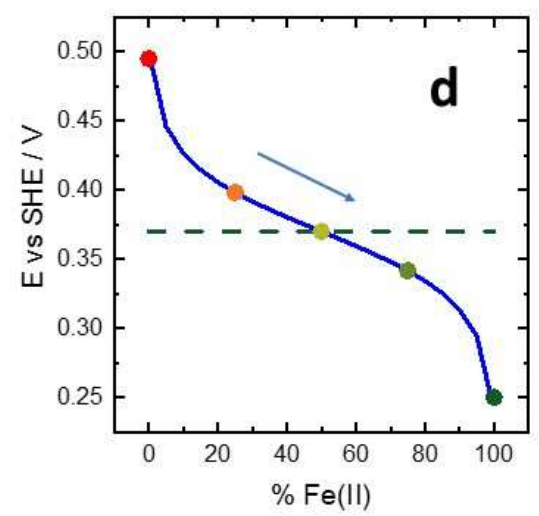
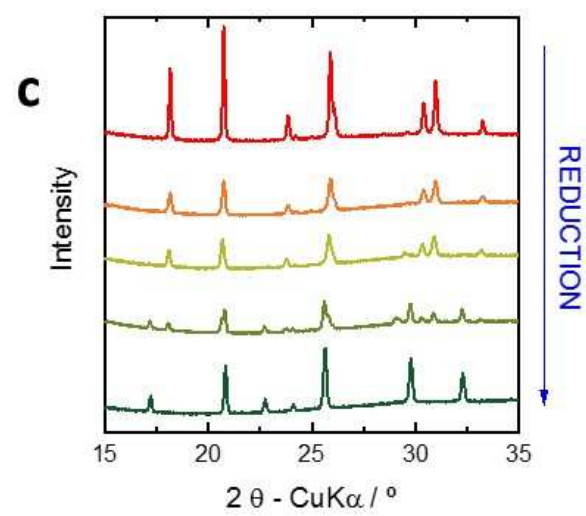
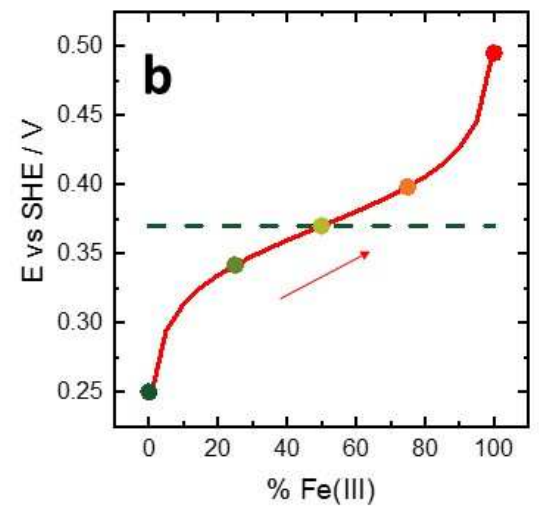
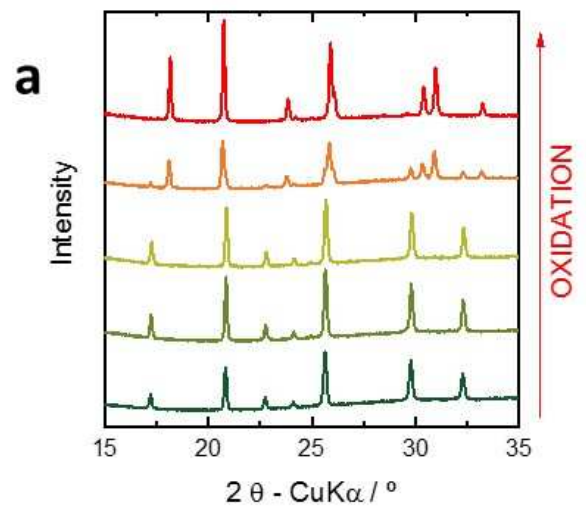


Figure 5

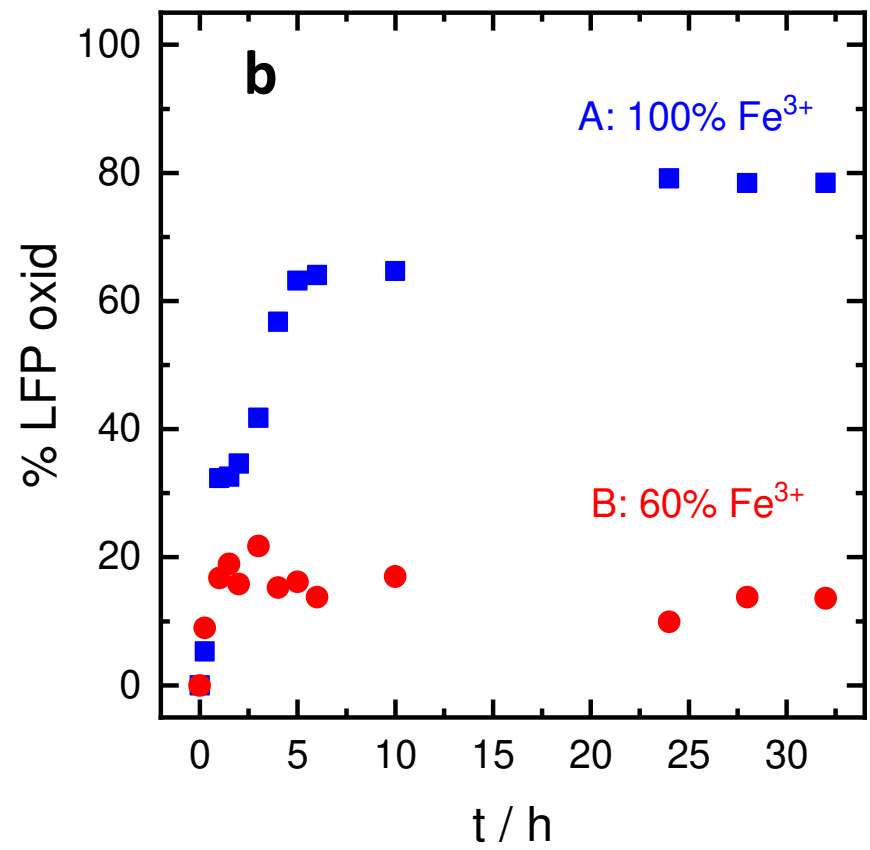
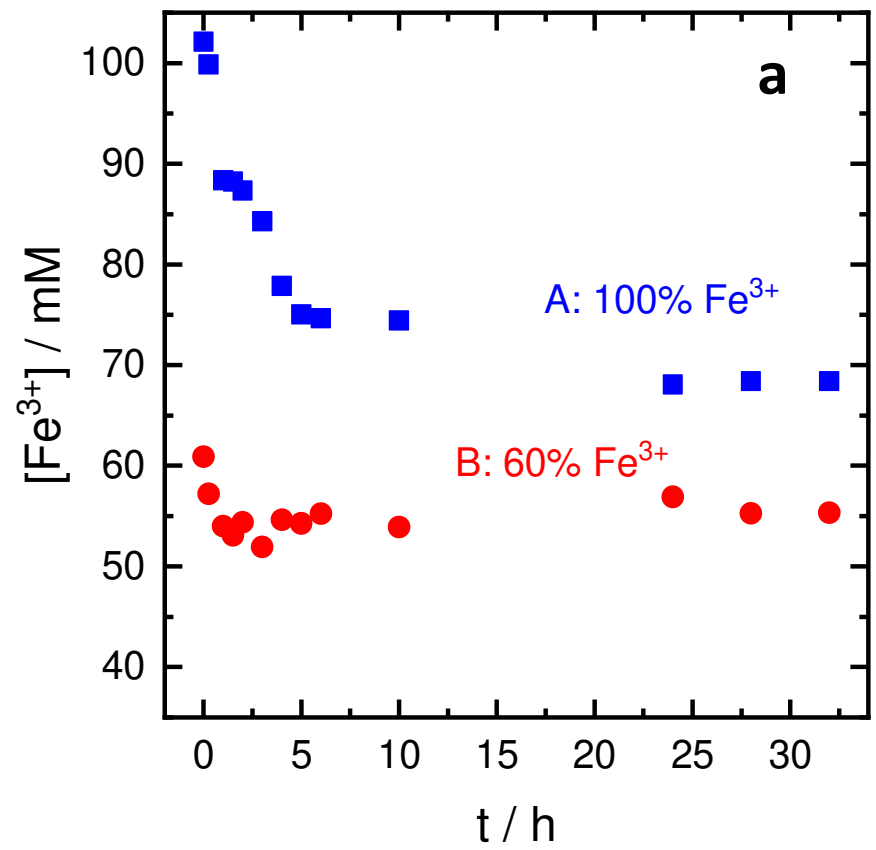


Figure 6

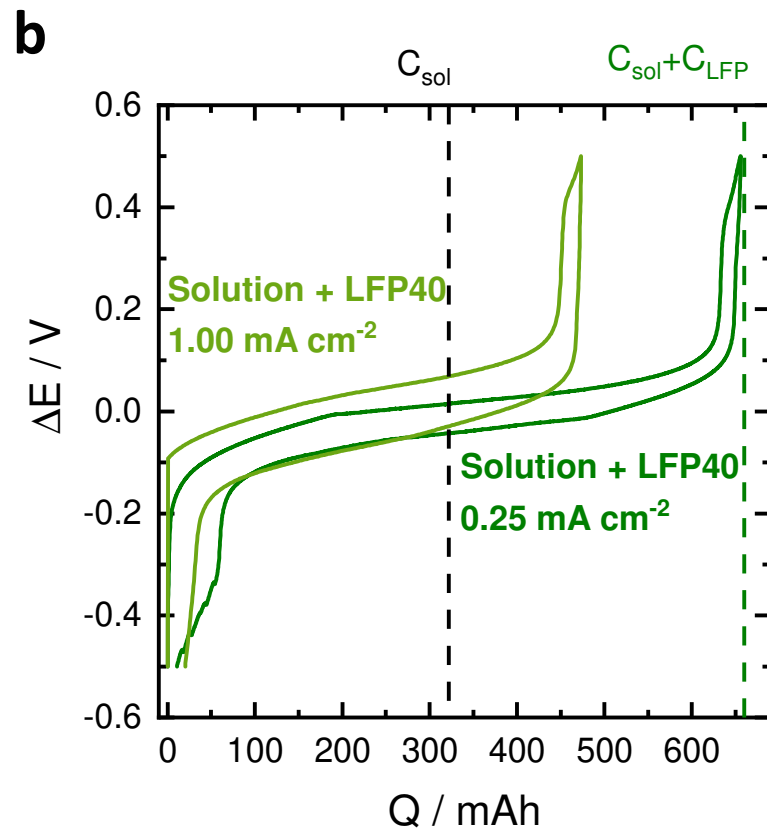
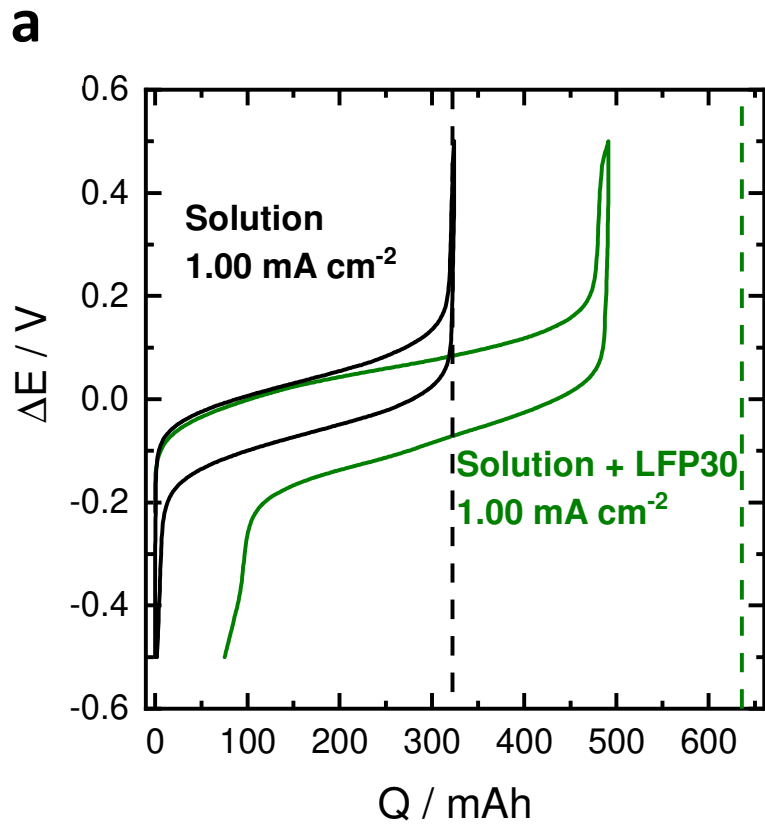


Figure 7

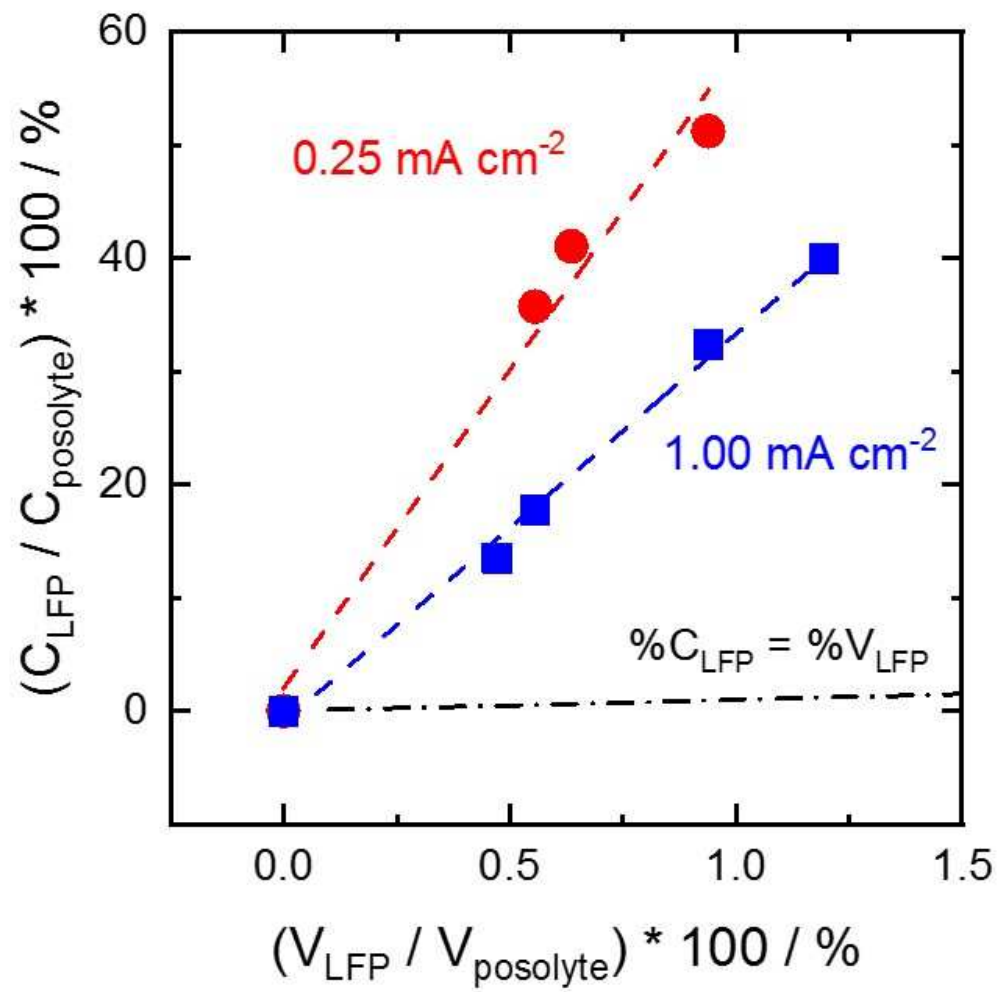


Figure 8

Sample	$\rho_{\text{theor.}}$ $\text{g}\cdot\text{cm}^{-3}$	$\rho_{\text{app.}}$ $\text{g}\cdot\text{cm}^{-3}$	Porosity (%)
LFP30NaCl	3.11	2.83 ± 0.08	9 ± 2
LFP30	3.51	2.25 ± 0.06	36 ± 2
LFP40NaCl	2.97	2.63 ± 0.11	12 ± 4
LFP40	3.51	1.85 ± 0.08	47 ± 2

Table 1

Type of posolyte	m_{LFP} g	Current density mA cm⁻²	Q_{theor} mAh	Q_{ch} mAh	% active LFP	Q_{dis} mAh	Q. Ef. %
Fe(CN) ₆ ^{3/4-}	0	1.00	322	324	0	322	~100
Fe(CN) ₆ ^{3/4-} + LFP30	1.85	1.00	636	491	54	416	85
Fe(CN) ₆ ^{3/4-} + LFP40	2.00	1.00	660	473	45	453	96
	2.00	0.25	660	656	99	647	99

Table 2

Graphical Abstract

